Available online at www.sciencedirect.com
ScienceDirect
Trans. Nonferrous Met. Soc. China 30(2020) 2435−2448
Transactions of Nonferrous Metals Society of China
www.tnmsc.cn

Characterization of grain growth behaviors by BP-ANN and Sellars models for nickle-base superalloy and their comparisons

Guo-zheng QUAN[1], Pu ZHANG[1], Yao-yao MA[1], Yu-qing ZHANG[1], Chao-long LU[1], Wei-yong WANG[2]

1. School of Material Science and Engineering, Chongqing University, Chongqing 400044, China;
2. School of Civil Engineering, Chongqing University, Chongqing 400045, China

Received 9 November 2019; accepted 8 July 2020

Abstract: In order to deeply understand the grain growth behaviors of Ni80A superalloy, a series of grain growth experiments were conducted at holding temperatures ranging from 1223 to 1423 K and holding time ranging from 0 to 3600 s. A back-propagation artificial neural network (BP-ANN) model and a Sellars model were solved based on the experimental data. The prediction and generalization capabilities of these two models were evaluated and compared on the basis of four statistical indicators. The results show that the solved BP-ANN model has better performance as it has higher correlation coefficient (r), lower average absolute relative error (AARE), lower absolute values of mean value (μ) and standard deviation (ω). Eventually, a response surface of average grain size to holding temperature and holding time is constructed based on the data expanded by the solved BP-ANN model, and the grain growth behaviors are described.

Key words: grain growth model; BP artificial neural network; Sellars model; average grain size

1 Introduction

In the hot deformation processes of nickel-based alloys, grain growth is a main microstructure evolution mechanism that cannot be ignored [1,2]. Aiming to characterize grain growth behaviors, a large number of works have paid attentions to developing various empirical models such as Beck model [3], Arrhenius model [4], Sellars model [5], Anelli model, and Sellars−Anelli model [6,7]. In Beck model and Arrhenius model, only one influence factor of average grain size, i.e., holding time or holding temperature, is considered, so that such models can only characterize the grain growth behaviors at a constant holding temperature or a constant holding time. In Sellars model, Anelli model and Sellars−Anelli model, two influence factors, i.e., holding time and holding temperature, are considered, so that these models describe the grain growth behaviors more accurately, and even achieve wide applications. However, the solutions of a series of coefficients in these empirical models need many experimental data, which limits their application.

In recent years, artificial neural network (ANN), and its improved form, back propagation artificial neural network (BP-ANN), as computational tools based on the operation of biological systems, have more and more applications in mapping various nonlinear relationships and predicting the data under unknown conditions [8−17]. It is worth noting that ANN doesn't need an explicit expression, and is

Foundation item: Project (cstc2018jcyjAX0459) supported by Chongqing Basic Research and Frontier Exploration Program, China; Projects (2019CDQYTM027, 2019CDJGFCL003) supported by the Fundamental Research Funds for the Central Universities, China

Corresponding author: Guo-zheng QUAN; Tel: +86-15922900904; E-mail: quangz2000@sina.com

DOI: 10.1016/S1003-6326(20)65390-0

motivated to address the different aspects of learning, inducing and deducing. That is to say, ANN can help draw conclusions from case observations and address the issues of prediction and interpretation. There have been a lot of reports dealing with the applications of ANN in predicting flow stress, and these works reveal that ANN is an effective method to describe the nonlinear behaviors in material field [9−13]. However, few attentions were paid to the applications of ANN in characterizing the grain growth behaviors.

In this work, BP-ANN method was introduced to characterize the grain growth behaviors of Ni80A nickel-based alloy. A series of grain growth experiments under different holding temperatures (1223−1423 K) and different holding times (0−3600 s) were conducted on M.MF.03000 numerical-controlled furnace. According to the experimental results of grain size, a BP-ANN model considering holding temperature and holding time as the input variables, and average grain size as the output variable, was solved. Meanwhile, a classical empirical model, Sellars model, was solved for comparisons. Subsequently, the performance of two models were evaluated by a series of standard statistical indicators including correlation coefficient (r), average absolute relative error (AARE), mean value (μ) and standard deviation (ω). Finally, the influence of holding temperature and holding time on grain size was uncovered by a response surface constructed based on the expanded data by the solved BP-ANN model.

2 Experimental

The chemical compositions of Ni80A are (in wt.%) 20.87 Cr, 2.07 Ti, 1.26 Fe, 0.68 Al, 0.63 Mn, 0.55 Si, 0.069 C, 0.01 S, and balanced Ni. The as-received material here is an as-forged billet with a diameter of 300 mm after homogenizing annealing. Thirty-five specimens with a diameter of 10 mm and a height of 12 mm were machined through wire-electrode cutting process from the as-received material. The heat treatment experiments were carried out in a numerical-controlled furnace with holding temperatures of 1223, 1273, 1323, 1373 and 1423 K and holding times of 0, 600, 1200, 1800, 2400, 3000 and 3600 s. After isothermal heating experiments, all the specimens were quenched by water immediately. To meet the needs of microstructural observations, the specimens were sectioned symmetrically by wire-electrode cutting. The cutting surfaces were polished mechanically and etched in a solution of HCl (100 mL), H_2SO_4 (5 mL) and $CuSO_4$ (5 g) at room temperature for 60 s. Subsequently, the microstructures in the section center were observed with the metallographic microscope, following which statistical analysis of grain size was conducted by the image analysis software of Image-Pro Plus. The average grain size was determined from a lot of individual grains by the method of linear intercept according to the ASTM standard E112 [18]. The original microstructure of the as-received specimen is almost homogeneous with an average size of 34.8 μm, as shown in Fig. 1.

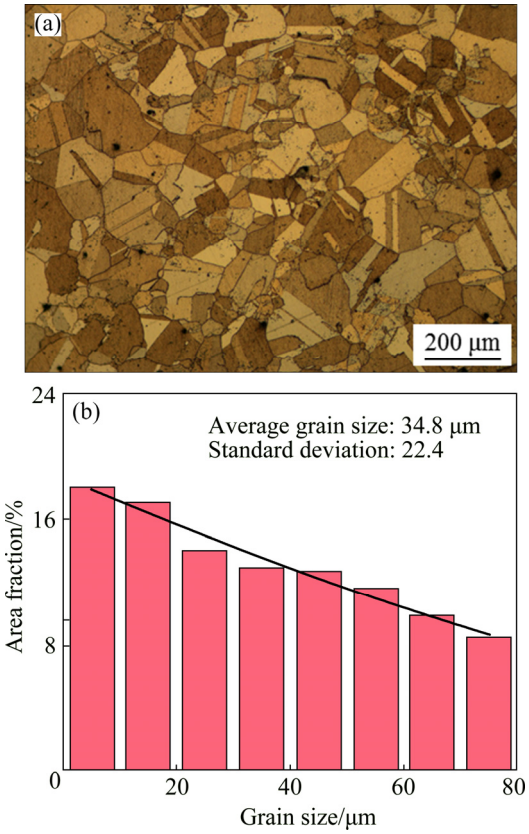

Fig. 1 Original microstructure of Ni80A (a) and histogram of grain size (b)

3 Results and discussion

3.1 Description of average grain size evolution by statistical analysis

Figures 2−6 represent the microstructures of Ni80A heated at different holding temperatures and holding time. They obviously indicate normal grain

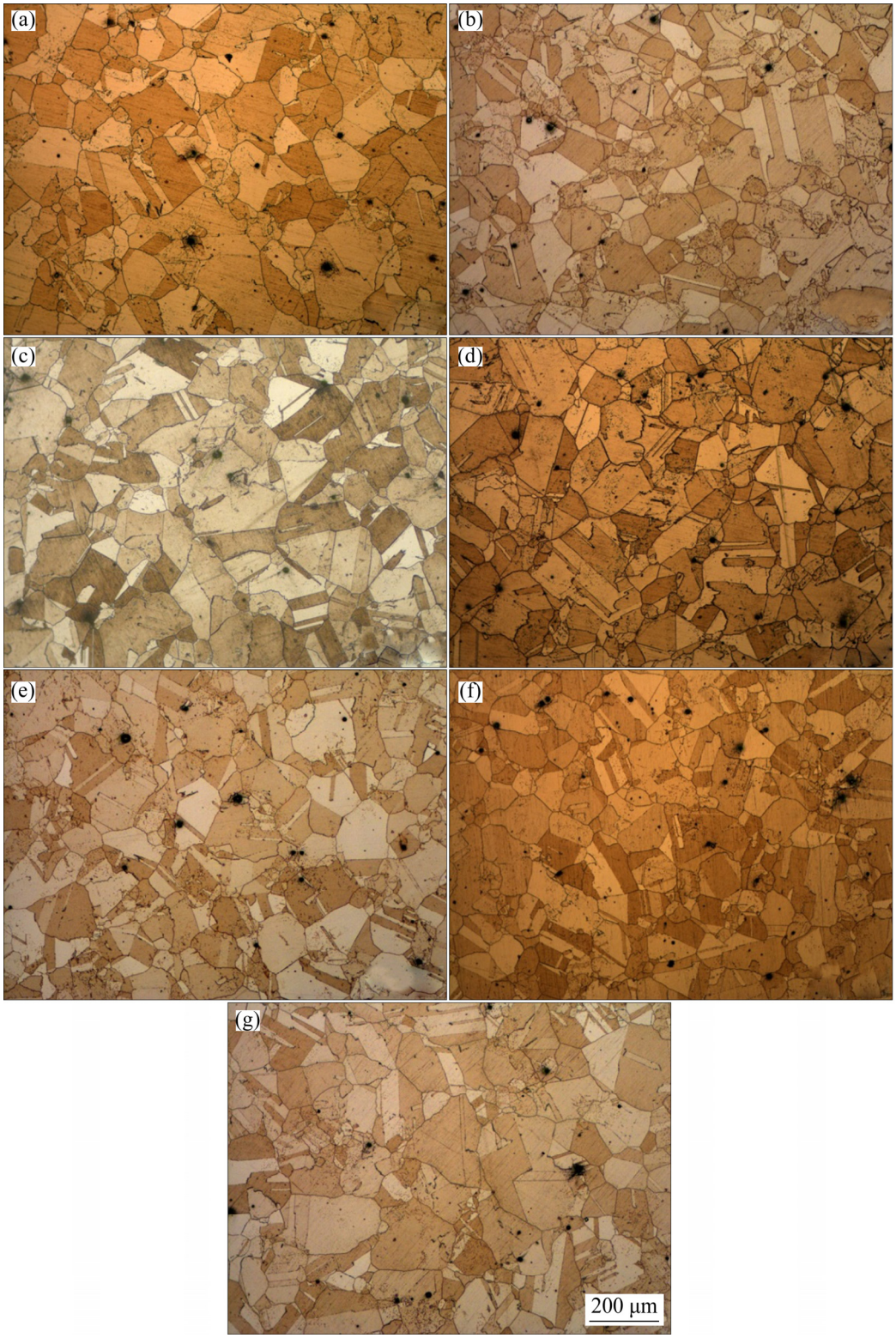

Fig. 2 Microstructural evolution of Ni80A during heating at 1223 K for different holding time: (a) 0 s; (b) 600 s; (c) 1200 s; (d) 1800 s; (e) 2400 s; (f) 3000 s; (g) 3600 s

growth behaviors with grain boundaries becoming straight and adjacent grain boundary angle being close to 120°. A few lamella-like straight annealing twins are found among the main equiaxial grains induced by static recrystallization. The average grain sizes at different holding temperatures and holding time are counted statistically, as listed in Table 1. It is summarized that the original grains

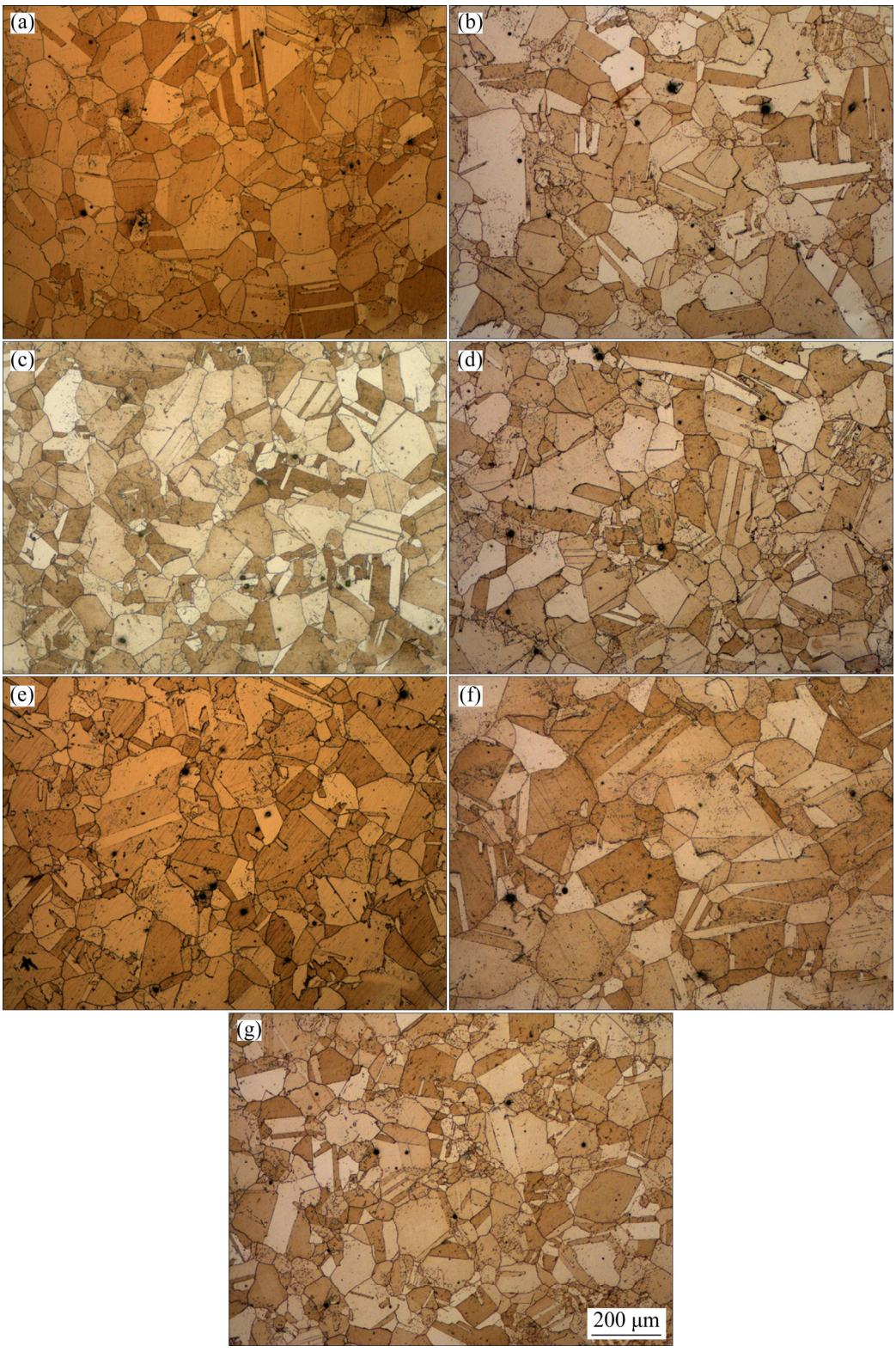

Fig. 3 Microstructural evolution of Ni80A during heating at 1273 K for different holding time: (a) 0 s; (b) 600 s; (c) 1200 s; (d) 1800 s; (e) 2400 s; (f) 3000 s; (g) 3600 s

have grown up obviously from average size of 34.8 μm to a high value.

3.1.1 Influence of holding temperature

In order to further uncover the influence of holding temperature on average grain size, the variations of average grain size with holding temperature at different holding time are plotted in Fig. 7. It is shown that a fitting curve at a certain

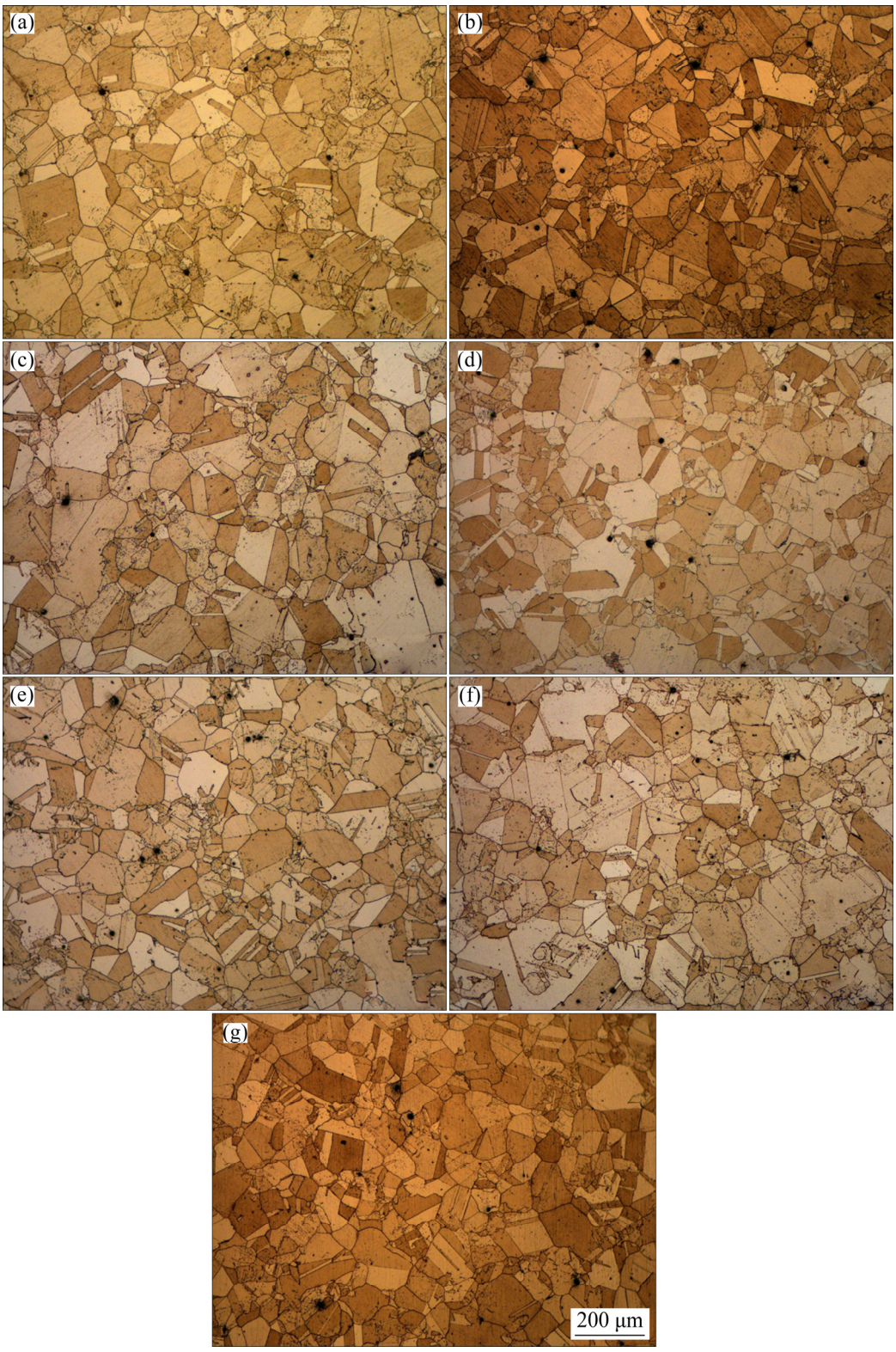

Fig. 4 Microstructural evolution of Ni80A during heating at 1323 K for different holding time: (a) 0 s; (b) 600 s; (c) 1200 s; (d) 1800 s; (e) 2400 s; (f) 3000 s; (g) 3600 s

holding time exhibits the significant characteristics of quadratic function. The grain growth rate increases gradually with the increase of holding temperature. Grain growth rate is related to the speed of grain boundary migration [1]. High temperature can promote the grain boundary migration. However, the presence of precipitates/ carbides in the Ni80A involving Gamma prime

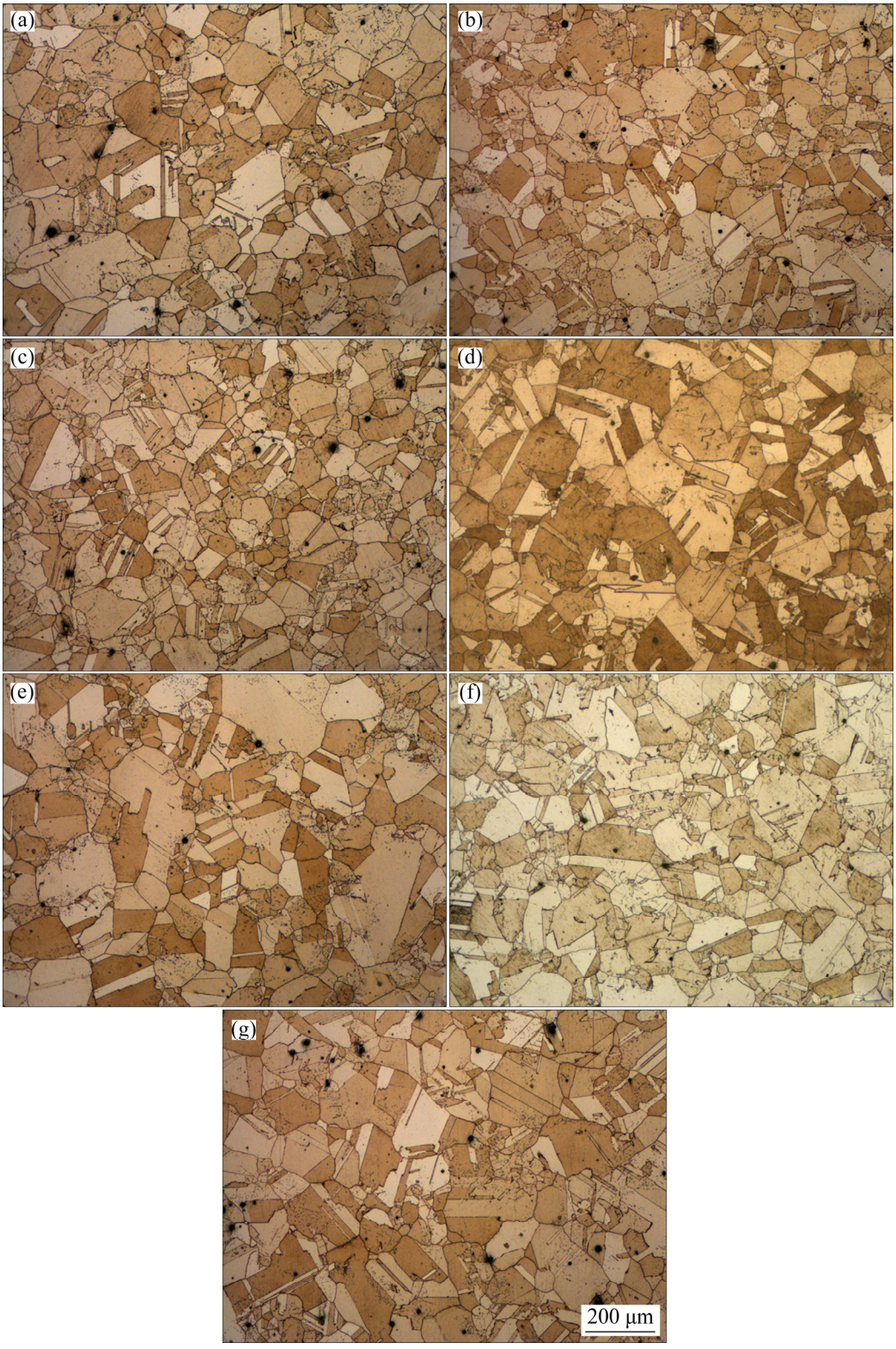

Fig. 5 Microstructural evolution of Ni80A during heating at 1373 K for different holding time: (a) 0 s; (b) 600 s; (c) 1200 s; (d) 1800 s; (e) 2400 s; (f) 3000 s; (g) 3600 s

phase, $M_{23}C_6$, M_7C_3 and MC, have great effects on grain boundaries such as hindering the grain boundary migration, and restricting the grain growth [19]. Table 2 gives the solvus temperature of precipitates/carbides in Ni80A [20]. The effect of restriction decreases gradually with the increase of holding temperature, since the precipitates/carbides are gradually dissolved over time. This is the reason

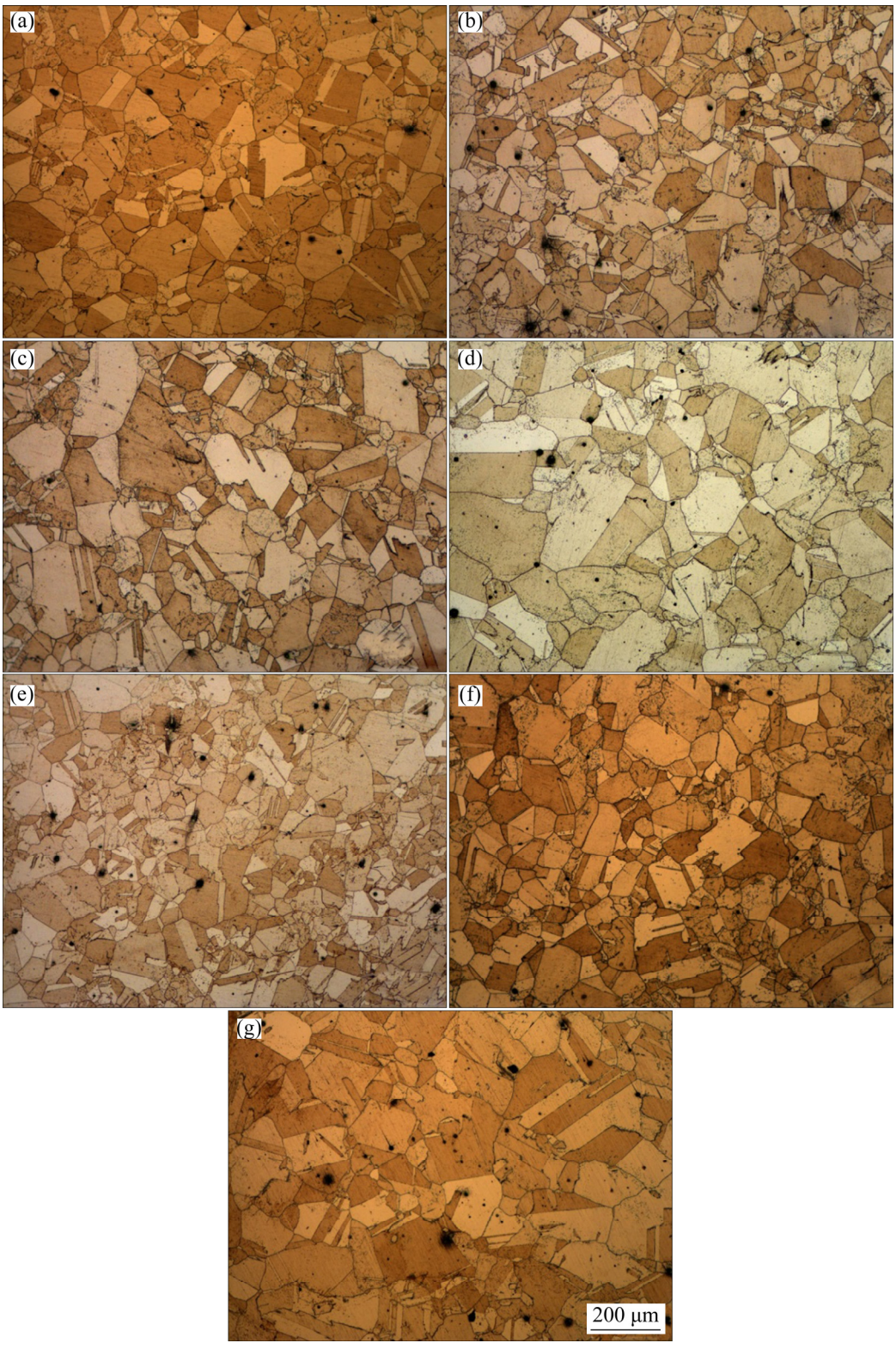

Fig. 6 Microstructural evolution of Ni80A during heating at 1423 K for different holding time: (a) 0 s; (b) 600 s; (c) 1200 s; (d) 1800 s; (e) 2400 s; (f) 3000 s; (g) 3600 s

why the grain growth rate increases gradually.

3.1.2 Influence of holding time

In order to further uncover the influence of holding time on average grain size, the variations of average grain size with holding time at different holding temperatures are plotted in Fig. 8. It is shown that a fitting curve at a certain holding temperature exhibits the significant characteristics

Table 1 Average grain size and corresponding standard deviation under different heating conditions (μm)

Holding time/s	Holding temperature/K				
	1223	1273	1323	1373	1423
0	137.6±56.6	141.9±56.9	146.2±56.4	149.6±55.7	161.6±53.8
600	141±56.7	145.9±56.2	152.9±55.1	164.5±53.3	172.4±49.1
1200	143.1±56.3	150.4±55.2	156.2±54	172.4±49.6	186.8±44.3
1800	148.6±55.8	153.6±54.6	161.4±52	177.1±45.9	196.1±37.9
2400	148.8±55.6	159.7±52.8	164.2±51	179.6±43	202.1±36.2
3000	149.4±55.4	160.1±52.7	165.9±50.3	186.4±36.2	204.9±36.9
3600	149.2±55.9	163.6±51.7	171.3±46.8	186.2±35.6	205.5±36.1

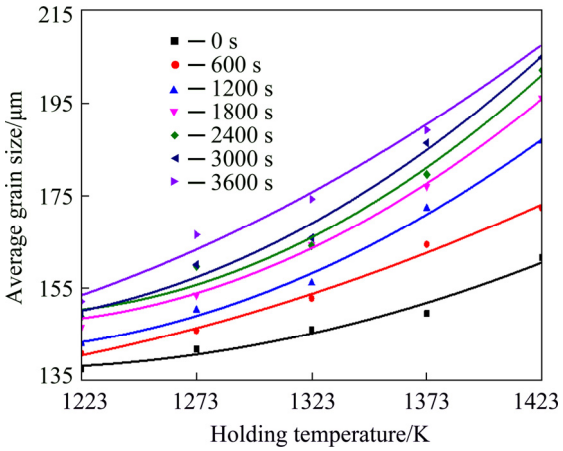

Fig. 7 Variations of average grain size with holding temperature at different holding time

Table 2 Solvus temperature of different phases in Ni80A

Phase	Solvus temperature/K
γ	>1223
$M_{23}C_6$	1323−1368
M_7C_3	1368−1423
MC	<1523

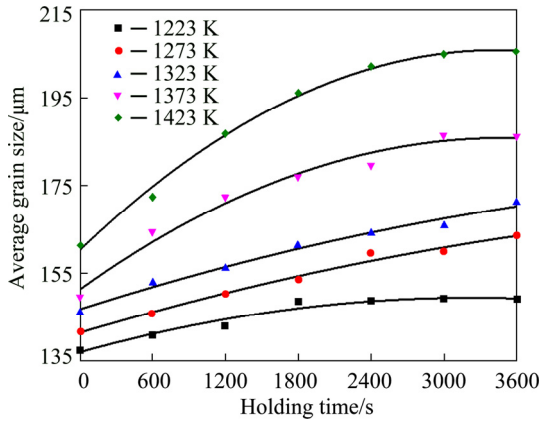

Fig. 8 Variations of average grain size with holding time at different holding temperatures

of parabolic function. It can be seen that with increasing holding time, average grain size increases gradually, while grain growth rate slows down. This is because grain growth is featured by grain boundary migration, a time-exhausting process. Long holding time facilitates the sufficient movement of grain boundaries. However, under the limited driven force, the further migration of grain boundaries becomes difficult with increasing holding time. Therefore, average grain size is little altered with further increase of holding time. Similar results have been obtained in Refs. [2,21].

3.2 Modeling average grain size evolution by physical method

In order to obtain the quantitative relationships among grain size, holding time and holding temperature, a classical grain growth model, Sellars model, is used to describe the grain size evolution of Ni80A [5], which is given as follows:

$$d^m = d_0^m + At\exp[-Q_{gg}/(RT)] \quad (1)$$

where d is average grain size, d_0 is initial grain size, Q_{gg} is grain growth activation energy, A and m are material constants, R is the gas constant (8.314 J/(mol·K)), T is the holding temperature, and t is the holding time.

Under given t and m, d is only determined by T. Taking natural logarithms on both sides of Eq. (1), Q_{gg} can be calculated as follows:

$$Q_{gg} = -R\left.\frac{\partial \ln(d^m - d_0^m)}{\partial(1/T)}\right|_t \quad (2)$$

However, it is difficult for conventional

numerical analysis methods to solve these constant values since m is unknown. In this work, m is assumed to be determined value (1, 2, 3, 4, 5, 6, 7, 8, 9 and 10), and then other constant values corresponding to each assumed m can be calculated. Furthermore, MSE as Eq. (3) is introduced to evaluate the accuracy of Eq. (1) under different assumed m, as illustrated in Table 3.

$$\mathrm{MSE}=\frac{1}{N}\sum_{i=1}^{N}(E_i-P_i)^2 \tag{3}$$

where E_i is the experimental value, P_i is the predicted value, and N is the number of samples.

Table 3 MSE corresponding to different m

m	MSE	m	MSE
1	56.98	6	8.77
2	34.02	7	12.77
3	19.53	8	22.06
4	14.62	9	34.89
5	10.68	10	49.48

Figure 9 illustrates the nonlinear relationship between MSE and m. The relationship can be represented as follows:

$$\mathrm{MSE}=103.889-63.434m+19.914m^2-3.534m^3+0.323m^4-0.011m^5 \tag{4}$$

In Eq. (4), with the increase of m, the MSE decreases to a valley value and then increases. When m is equal to 5.6174, the valley value of MSE can be reached.

Substituting m into Eq. (2), the curves of $\ln(d^m-d_0^m)$ vs $-1/(RT)$ can be plotted under different holding times, as shown in Fig. 10. The mean slope of these curves is calculated as Q_{gg}, which is equal to 206004 J/mol. At the same time, A can be calculated to be 3.993×10^{17}.

Substituting aforementioned constants into Eq. (1), Sellars model of Ni80A is solved as follows:

$$d^{5.6174}=d_0^{5.6174}+3.993\times10^{17}t\cdot\exp[-206004/(8.314T)] \tag{5}$$

To verify the validity of Sellars model, a comparison of the model predictions and experimental measurements is demonstrated in Fig. 11. Results show the correlation coefficient (r) of solved Sellars model. r close to 1 indicates that the calculated average grain sizes are in agreement with the experimental data.

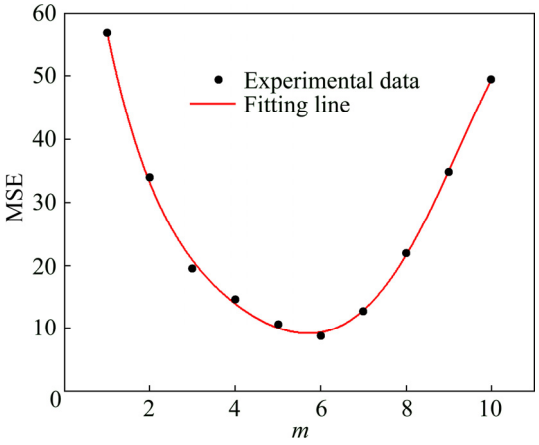

Fig. 9 Relationships between MSE and m

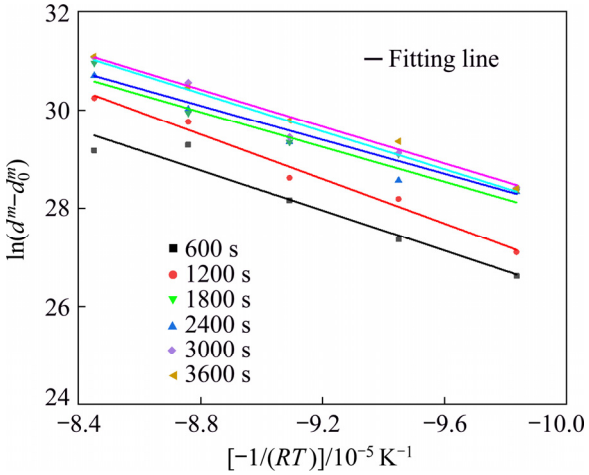

Fig. 10 The relationships between $\ln(d^m-d_0^m)$ and $-1/(RT)$

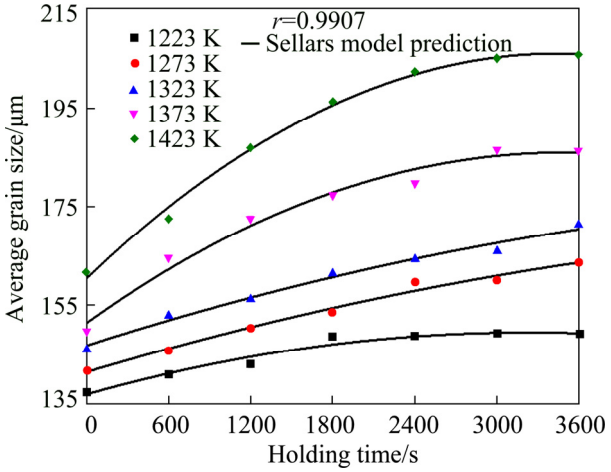

Fig. 11 Comparison of Sellars model and measured values of grain growth

3.3 Modeling average grain size evolution by BP-ANN method

BP-ANN is a multilayer feed forward network trained by the backward propagation learning algorithm. The structure of BP-ANN contains one input layer, one output layer and one or more hidden layers. The function of the input layer is to accept the output layer signal. The function of the output layer is to generate the output signal. The function of the hidden layer is to link input layer and output layer. In common, the sophisticated construction of BP-ANN includes the selection of appropriate transfer function and the design of the appropriate numbers of hidden layers and units in each layer. The ideal structure of BP-ANN consists of as few hidden layers and connections as possible, which is necessary to achieve a good approximation of the true function. The neurons number of hidden layer is usually determined by the designer's experience and a trail-and-error procedure. However, a network with fewer hidden units than the required number will not be able to learn the input and output mapping, and too many hidden units will not be able to summarize any unseen data [17]. To approach the proposed accuracy, at beginning, BP-ANN model is trained with only two neurons for each hidden layer, following which the neuron number is adjusted continually (three, four, etc) [16]. The process is repeated by changing the number of neurons. Finally, one hidden layer and four neurons in hidden layer are favorable enough for the final network architecture. As an empirical fact, "trainbr" function and "learngd" function are selected as the training function and learning function, respectively. Meanwhile, the selected transfer function is "Tansig" for hidden layer, whereas "Purelin" for output layer.

In this work, input layer units correspond to T and t, and output layer units correspond to d. The schematic structure of BP-ANN is shown in Fig. 12. The total thirty-five grain size datasets are divided into training dataset and independent test dataset. The training dataset includes the experiment data at 1223, 1273, 1373 and 1423 K. The left experiment data are considered as test dataset to test the BP-ANN work performance.

As given in Table 1, holding temperatures vary from 1223 to 1423 K, holding times vary from 0 to 3600 s, and average grain size vary from 139.1 to 205.5 μm. To eliminate the arbitrary influence of similarity between the objects and speed up the convergence of the training network, dimensionless normalization of all dataset must be carried out. The normalization equation is given as follows:

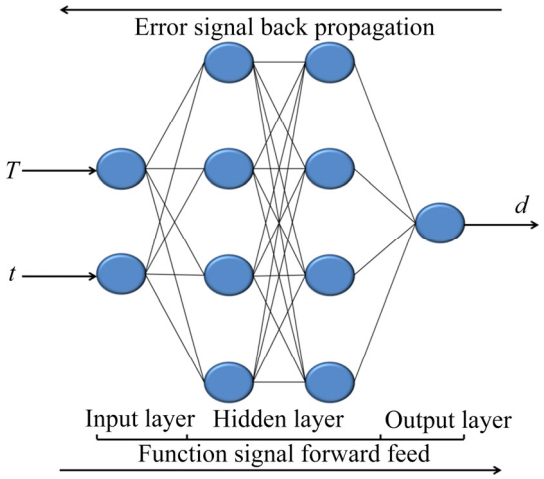

Fig. 12 Schematic of BP-ANN architecture

$$X_n = 0.05 + 0.25 \times \frac{X - 0.95X_{\min}}{1.05X_{\max} - 0.95X_{\min}} \tag{6}$$

where X is the initial data of input or output variable; $X_{\min}$, $X_{\max}$ and X_n are the minimum value of X, the maximum value of X and the value of X after normalization processing, respectively.

In addition, the network adopts an evaluator, the sum of squared errors (SSE) [22,23], to evaluate the ability of the BP-ANN training model. The function of SSE can be defined as follows:

$$\mathrm{SSE} = \sum_{i=1}^{N} (E_i - P_i)^2 \tag{7}$$

Here, the proposed accuracy, i.e., the maximum *SSE*, is set to be 0.001. This work is done by the Neural Network Toolbox.

By the well-trained BP-ANN model, the grain sizes under different experiment conditions are predicted. Figure 13 shows the comparisons between the average grain size values predicted by the solved BP-ANN model and the experimental grain size, which indicates that the solved BP-ANN model can effectively grasp the evolution of the average grain size.

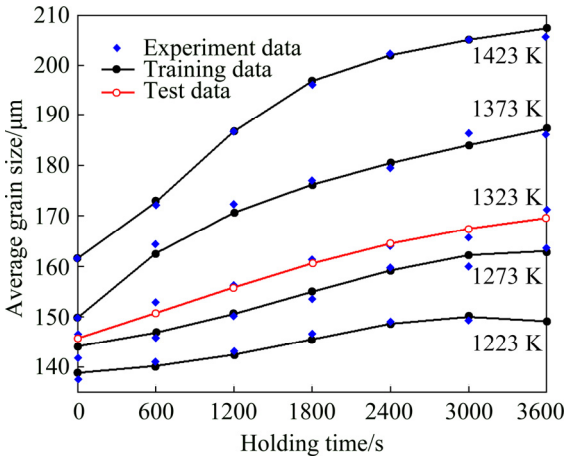

Fig. 13 Comparisons of BP-ANN prediction values with experimental values under different experiment conditions

3.4 Prediction capability comparison between BP-ANN model and Sellars model

To evaluate the prediction accuracy of BP-ANN model and Sellars model, three statistical indicators including relative error (δ), average absolute relative error (AARE) and correlation coefficients (r) are introduced into this work. δ expressed by Eq. (8) represents the ratio of the prediction error to the experimental value. AARE expressed by Eq. (9) represents the average value of the unsigned error. r expressed by Eq. (10) represents the degree of linear correlation among variables. it is worth pointing out that higher r, lower AARE and lower absolute value of δ indicate higher prediction accuracy:

$$\delta = \frac{P_i - E_i}{E_i} \times 100\% \tag{8}$$

$$\text{AARE} = \frac{1}{N}\sum_{i=1}^{N}\left|\frac{P_i - E_i}{E_i}\right| \times 100\% \tag{9}$$

$$r = \frac{\sum_{i=1}^{N}(E_i - \bar{E})\sum_{i=1}^{N}(P_i - \bar{P})}{\sqrt{\sum_{i=1}^{N}(E_i - \bar{E})^2 \sum_{i=1}^{N}(P_i - \bar{P})^2}} \tag{10}$$

where $\bar{E}$ and $\bar{P}$ are the mean values of experimental values and predicted values, respectively.

The calculation results show that as for BP-ANN model, δ varies from −2.22% to 1.53%; whereas as for Sellars model, it varies from −3.32% to 3.37%. Figure 14 shows the correlation relationships between the experimental values and predicted values by BP-ANN model and Sellars model, respectively. The r values of BP-ANN model and Sellars model are 0.9982 and 0.9907, respectively. The AARE values of BP-ANN model and Sellars model are 0.52% and 1.45%, respectively. It can be concluded that BP-ANN model relative to Sellars model has higher r and lower AARE.

In order to further evaluate the accuracy of BP-ANN model and Sellars model, the distribution of δ is analyzed, as shown in Fig. 15, in which the histogram height represents the relative frequency of δ. The histogram distribution exhibits a characteristic of typical Gaussian function as Eq. (11). In Eq. (11), the indicator of mean value (μ) as Eq. (12) reflects the central tendency, and the indicator of standard deviation (ω) as Eq. (13) reflects the discrete degree of dispersion. Here, the μ and ω of Sellars model are −0.62235% and

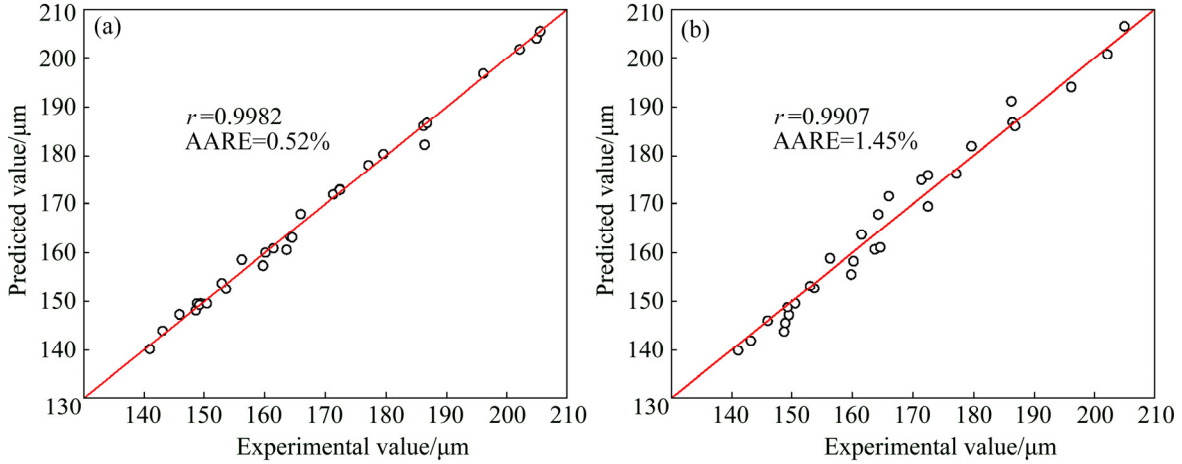

Fig. 14 Correlation between predicted and experimental values for BP-ANN model (a) and Sellars model (b)

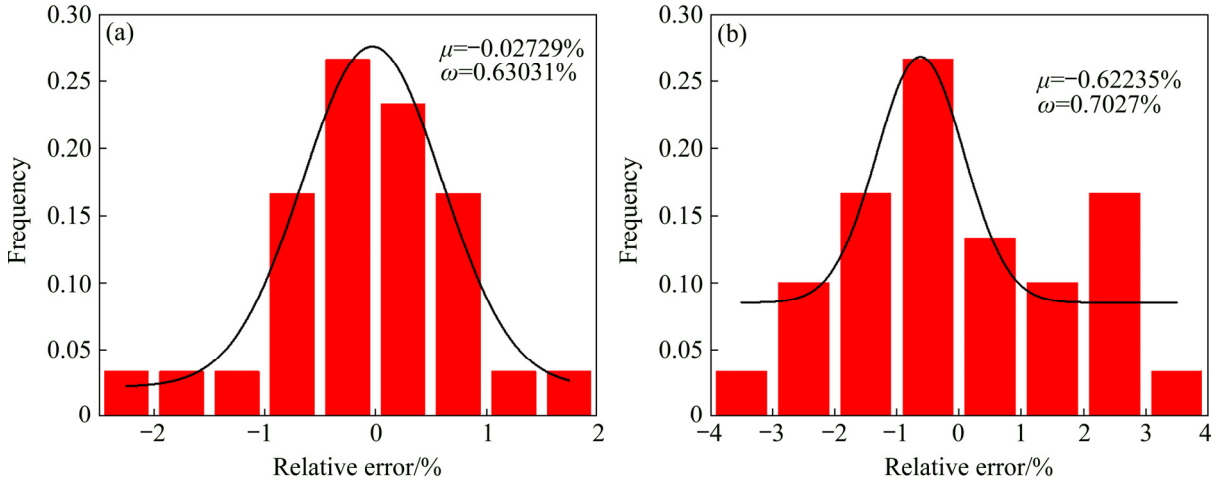

Fig. 15 Distribution of relative errors on grain size predicted by BP-ANN model (a) and Sellars model (b) relative to experimental ones

0.7027%, while the μ and ω of BP-ANN model are −0.02729% and 0.63031%. It can be concluded that the distribution of δ obtained from the BP-ANN model is more concentrated.

$$y = y_0 + A\exp\left[\frac{(\delta_i - \mu)^2}{-2\mu^2}\right] \tag{11}$$

$$\mu = \frac{1}{N}\sum_{i=1}^{N}\delta_i \tag{12}$$

$$\omega = \sqrt{\frac{1}{N-1}\sum_{i=1}^{N}(\delta_i - \mu)^2} \tag{13}$$

where δ_i is the value of relative error; y_0 and A are constants, and here N=30.

3.5 Prediction potentiality of BP-ANN model

It is worth pointing out that the average grain size of samples heat-treated at 1323 K, as the test dataset, did not participate in the training process of BP-ANN model, whereas all the grain size participate in the solving process of Sellars model. The comparisons of δ, AARE, r, μ and ω for BP-ANN model and Sellars model show that the former has higher prediction accuracy. In another word, BP-ANN model achieves higher learning ability while it needs less data to participate in the model construction. Subsequently, BP-ANN model was applied in expanding the average grain size at different holding temperatures (1223−1423 K) and holding times (0−3600 s). Based on the expanding data, a response surface of average grain size to holding temperature and holding time, is constructed, as shown in Fig. 16. Consequently, the correspondence relationships among grain size, holding temperature and holding time are mapped.

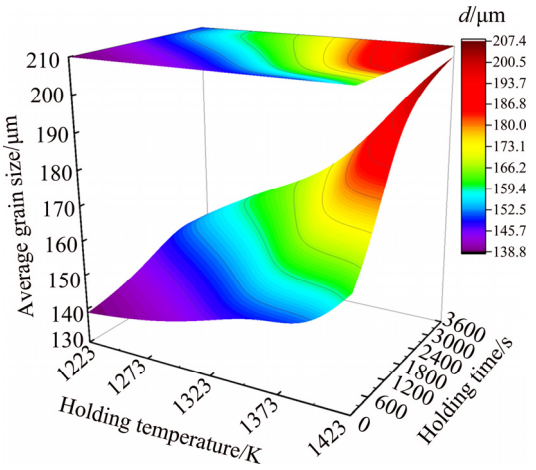

Fig. 16 Response surface of average grain size on holding temperature and holding time

4 Conclusions

(1) A Sellars model is solved. The activation energy of grain growth of Ni80A is calculated to be 206004 J/mol. A BP-ANN model taking holding temperature (T) and holding time (t) as the input variables, and average grain size (d) as the output variable is constructed.

(2) r, AARE, μ and ω of BP-ANN model are 0.9982, 0.52%, −0.02729% and 0.63031%, respectively, while these indicators of Sellars model

are 0.9907, 1.45%, −0.62235% and 0.7027%, respectively. Higher r, lower AARE, lower absolute values of μ and ω indicate that BP-ANN has higher prediction accuracy.

(3) A response surface of average grain size to holding temperature and holding time is constructed. Then, the corresponding relationships among grain size, holding temperature and holding time are mapped.

References

[1] RANDLE V, RIOS P R, HU Y. Grain growth and twinning in nickel [J]. Scripta Materialia, 2008, 58(2): 130−133.

[2] CHEN Xiao-ming, LIN Yong-cheng, WU Fan. EBSD study of grain growth behavior and annealing twin evolution after full recrystallization in a nickel-based superalloy [J]. Journal of Alloys and Compounds, 2017, 724: 198−207.

[3] BECK P A, HOLZWORTH M L, HU H. Instantaneous rates of grain growth [J]. Physical Review, 1948, 73(5): 526−527.

[4] HILLERT M. On the theory of normal and abnormal grain growth [J]. Acta Metallurgica, 1965, 13(3): 227−238.

[5] SELLARS C M, WHITEMAN J A. Recrystallization and grain growth in hot rolling [J]. Metal Science, 1979, 13: 187−194.

[6] CHEN Li-qiang, SUI Feng-li, LIU Xiang-hua. Grain growth model of Inconel 718 alloy forged slab in reheating process prior to rough rolling [J]. Acta Metallurgica Sinica (Chinese Edition), 2009, 45(10): 1242−1248. (in Chinese)

[7] XU Yao-wen, TANG Di, SONG Yong, PAN Xiao-gang. Prediction model for the austenite grain growth in a hot rolled dual phase steel [J]. Materials and Design, 2012, 36: 275−278.

[8] BASHEER I A, HAJMEER M N. Artificial neural networks: Fundamentals, computing, design, and application [J]. Journal of Microbiological Methods, 2001, 43(1): 3−31.

[9] PHANIRAJ M P, LAHIRI A K. The applicability of neural network model to predict flow stress for carbon steels [J]. Journal of Materials Processing Tech, 2003, 141(2): 219−227.

[10] LIN Yong-cheng, ZHANG Jun, ZHONG Jue. Application of neural networks to predict the elevated temperature flow behavior of a low alloy steel [J]. Computational Materials Science, 2008, 43(4): 752−758.

[11] NAZARI A, TORGAL F P. Predicting compressive strength of different geopolymers by artificial neural networks [J]. Ceramics International, 2013, 39(3): 2247−2257.

[12] OZERDEM M S, KOLUKISA S. Artificial neural network approach to predict the mechanical properties of Cu–Sn–Pb–Zn–Ni cast alloys [J]. Materials and Design, 2009, 30(3): 764−769.

[13] YAN Jie, PAN Qing-lin, LI An-de, SONG Wen-bo. Flow behavior of Al−6.2Zn−0.70Mg−0.30Mn−0.17Zr alloy during hot compressive deformation based on Arrhenius and ANN models arametric optimization of dry sliding wear loss of copper−MWCNT composites [J]. Transactions of Nonferrous Metal Society of China, 2017, 27(3): 638−647.

[14] TAN Ye-fa, HE Long, WANG Xiao-long, HONG Xiang, WANG Wei-gang. Tribological properties and wear prediction model of TiC particles reinforced Ni-base alloy composite coatings [J]. Transactions of Nonferrous Metal Society of China, 2014, 24(8): 2566−2573.

[15] QUAN Guo-zheng, PU Shi-ao, ZHAN Zong-yang, ZOU Zhen-yu, LIU Ying-ying, XIA Yu-feng. Modelling of the hot flow behaviors for Ti−13Nb−13Zr alloy by BP-ANN model and its application [J]. International Journal of Precision Engineering and Manufacturing, 2015, 16(10): 2129−2137.

[16] QUAN Guo-zheng, WEN Hai-rong, PAN-Jia, ZOU Zhen-yu. Construction of processing maps based on expanded data by BP-ANN and identification of optimal deforming parameters for Ti−6Al−4V alloy [J]. International Journal of Precision Engineering and Manufacturing, 2016, 17(2): 171−180.

[17] QUAN Guo-zheng, ZHANG Zhi-hua, PAN Jia, XIA Yu-feng. Modelling the hot flow behaviors of AZ80 alloy by BP-ANN and the applications in accuracy improvement of computations [J]. Materials Research, 2015, 18(6): 1331−1345.

[18] ASTM Standard E112-17. Standard practice for calculating sample size to estimate, with specified precision, the average for a characteristic or a lot of process [S]. 2013.

[19] TIAN Bao-hui, ZICKLER G A, LIND C, PARIS O. Local microstructure and its influence on precipitation behavior in hot deformed Nimonic 80a [J]. Acta Materialia, 2003, 51(14): 4149−4160.

[20] VOICE W E, FAULKNER R G. Carbide stability in Nimonic 80a alloy [J]. Metallurgical Transactions A (Physical Metallurgy and Materials), 1985, 16(4): 511−520.

[21] CHEN Ming-song, ZOU Zong-huai, LIN Yong-cheng, LI Hong-bin, YUAN Wu-quan. Effects of annealing parameters on microstructural evolution of a typical nickel-based superalloy during annealing treatment [J]. Materials Characterization, 2018, 141: 212−222.

[22] CHAI Rong-xia, CHENG Guo, LI Yu. Two flowing stress models for hot deformation of XC45 steel at high temperature [J]. Materials Science and Engineering A, 2012, 534: 101−110.

[23] MANDAL S, RAKESH V, SIVAPRASAD P V, VENUGOPAL S, KASIVISWANATHAN K V. Constitutive equations to predict high temperature flow stress in a Ti-modified austenitic stainless steel [J]. Materials Science and Engineering A, 2009, 500(1−2): 114−121.

基于 BP-ANN 和 Sellars 模型的镍基高温合金晶粒长大行为表征及其比较

权国政[1]，张 普[1]，马遥遥[1]，张钰清[1]，鹿超龙[1]，王卫永[2]

1. 重庆大学 材料科学与工程学院，重庆 400044；
2. 重庆大学 土木工程学院，重庆 400045

摘 要：为了深入理解 Ni80A 的晶粒长大行为，在不同温度(1223~1423 K)和不同保温时间(0~3600 s)下进行一系列的晶粒长大实验。基于实验数据，建立 BP 神经网络并求解 Sellars 模型。使用 4 个统计指标比较和评价这两个模型的预测与泛化能力。结果表明，所建立的 BP 神经网络具有更高的 r 值、更低的 AARE 值、更低的绝对 μ 值和 ω 值。最后，基于求解的 BP 神经网络扩展的数据建立平均晶粒尺寸对保温温度和保温时间的响应面，并描述晶粒的长大行为。

关键词：晶粒长大模型；BP 神经网络；Sellars 模型；平均晶粒尺寸

(Edited by Bing YANG)